

Interacting type-II semi-Dirac quasiparticles

Mohamed M. Elsayed,¹ Taras I. Lakoba,² and Valeri N. Kotov¹

¹*Department of Physics, University of Vermont, Burlington, Vermont 05405, USA*

²*Department of Mathematics and Statistics, University of Vermont, Burlington, Vermont 05405, USA*

Type-II semi-Dirac fermions in two dimensions have been proposed to describe topologically non-trivial low energy excitations in titanium/vanadium oxide heterostructures. These quasiparticles appear at the merger of three Dirac cones, resulting in a non-zero Berry phase. We find, by employing Hartree-Fock, renormalization group and RPA techniques, that the spectrum is very sensitive to long-range electron-electron interactions and can undergo a profound transformation. Specifically the quasiparticle spectrum evolves, driven by interactions, from anisotropic Dirac dispersion at the lowest energies, towards the characteristic type-II semi-Dirac boomerang shape as the energy increases. The corresponding density of states varies between linear and power one third ($\rho(\varepsilon) \sim |\varepsilon| \rightarrow |\varepsilon|^{1/3}$). The crossover scale is controlled by the interaction strength $\alpha = e^2/(\hbar v)$, and the specifics of the effective interacting Hamiltonian. Our results imply that various physical characteristics exhibit critical behavior with continuously varying 'critical exponents'; for example Landau levels in a magnetic field vary with the energy scale: $|\varepsilon_n(B)| \sim (nB)^{1/2} \rightarrow (nB)^{3/4}$, $n = 0, 1, 2, \dots$, and similarly for other observables.

Introduction— Semi-Dirac fermions are a hybrid low-energy excitation, exhibiting the qualities of both massless Dirac particles and massive Galilean particles at once. More precisely, they disperse linearly in a given direction in momentum space, and quadratically in the orthogonal direction. This is most easily understood as resulting from the merger of two Dirac cones at the critical point of a semimetal-insulator transition, whereby the Berry phases annihilate and the critical semi-Dirac spectrum emerges [1, 2]. Furthermore, there are other possible 'flavors' of semi-Dirac fermions. Higher order generalizations have attracted theoretical study, where the quadratic dispersion is generalized to an arbitrary even power law [3, 4]. Recently there has been a proposed lattice model realization for the most basic non-trivial case in this class of Hamiltonians, namely the quartic semi-Dirac fermions [5]. Moreover, there is an even more exotic flavor of semi-Dirac fermions that are not topologically trivial. These excitations emerge at a critical point where not two but three Dirac cones coalesce, producing a finite Berry phase and what has been dubbed a type-II semi-Dirac spectrum [6]. The dispersion retains its semi-Dirac character in the sense that it is still linear and quadratic along the given axes, but exhibits a different admixture of momentum components at intermediate angles [6, 7]. This symmetry reduced model was first proposed to reconcile the finite Chern number and semi-Dirac behavior of quasiparticles in titanium/vanadium oxide heterostructures [6]. However, it may also be realized in more conventional platforms such as bilayer graphene, by leveraging interlayer sliding [8, 9]. Such systems have been shown to exhibit a rich variety of topological phases that are accessible via fine tuning with light-matter interactions [10]. In addition, the peculiar anisotropy leads to highly unusual optical and transport properties [11]. Topological semi-metallic phases have also been analyzed in detail both experimen-

tally and theoretically in ZrSiS, reporting a measurement of the signature Landau level scaling with magnetic field [12].

Electron-electron interactions are known to have pronounced effects in ordinary semi-Dirac fermions [1, 13–16]. Short range interactions have been shown to stabilize modulated ordered phases in the charge, spin, and superconducting sectors around a quantum critical point [17, 18]. On the other hand, the long range Coulomb interaction produces two low energy regimes in which there is unusually strong spectrum renormalization [3, 19]. Motivated by these results, we study the spectrum renormalization of the topological type-II semi-Dirac fermions due to the long range, and RPA screened, Coulomb interaction. Remarkably, the interacting system hosts massless Dirac quasiparticles at the lowest energies, smoothly transitioning to the free fermionic behavior with increasing energy. This is captured in the exponent η of the density of states ($\rho(\varepsilon) \sim \varepsilon^{\eta(\varepsilon)}$) as a function of energy varying from 1 to 1/3 on a sigmoid. As a consequence, many other physical properties and observables will have a continuously evolving dependence on the energy scale of interest.

We consider the Hamiltonian describing type-II semi-Dirac fermions [6]:

$$\mathcal{H}(\mathbf{k}) = (g_1 k_x^2 - v k_y) \hat{\sigma}_x + g_2 k_x k_y \hat{\sigma}_y. \quad (1)$$

Such fermions can arise at the critical point of the transition shown in Figure 1. We rescale the momenta, defining $p_{x,y} = (g_1/v)k_{x,y}$, and introduce the energy scale $\varepsilon_0 = v^2/g_1$ to arrive at the dispersion

$$\varepsilon(\mathbf{p}) = \pm \varepsilon_0 \sqrt{(p_x^2 - p_y^2)^2 + (gp_x p_y)^2}, \quad (2)$$

where we define $g \equiv g_2/g_1$. A plot of the spectrum is shown in Figure 2 using a representative value of $g = 0.41$ as it is in the candidate material $(\text{TiO}_2)_5(\text{VO}_2)_3$ [6].

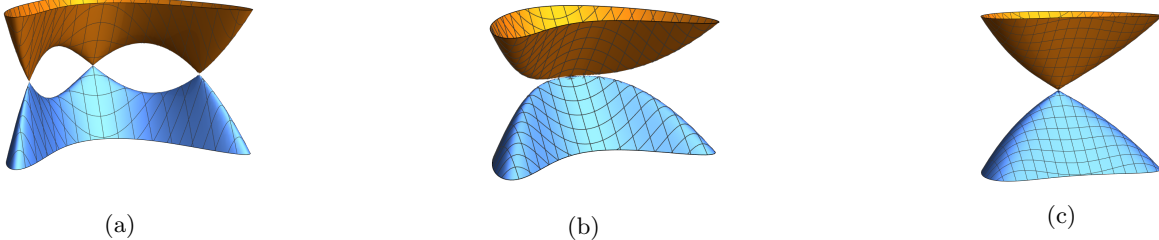


FIG. 1. Low energy dispersion corresponding to the Hamiltonian in Eq.(1) under a small perturbation Δ , such that $\mathcal{H} = (g_1 k_x^2 - v k_y + \Delta) \hat{\sigma}_x + g_2 k_x k_y \hat{\sigma}_y$. (a) $\Delta < 0$, leading to the presence of three Dirac cones located at $(0, \Delta/v), (\pm\sqrt{-\Delta g_1}, 0)$. (b) $\Delta = 0$: The three cones coalesce at the origin, giving rise to a type-II semi-Dirac point with a finite Berry phase. (c) $\Delta > 0$: The band crossing is shifted to $k_y = (g_1^2/vg_2)\Delta$. At the smallest momenta the spectrum is linear, but exhibits type-II semi-Dirac behavior at larger energies.

Energy Variables and Density of States— When calculating diagrams and other quantities of interest in systems with such anisotropy, it is useful to recast into energy-angle variables which we define as follows:

$$\begin{aligned} p_x^2 - p_y &= (\varepsilon/\varepsilon_0) \cos \varphi, \\ g p_x p_y &= (\varepsilon/\varepsilon_0) \sin \varphi. \end{aligned} \quad (3)$$

The solution of these equations in the low energy limit ($\varepsilon/\varepsilon_0 \ll 1$) is

$$\begin{aligned} p_x &= \text{sgn}(\sin \varphi) \left(\frac{E |\sin \varphi|}{g} \right)^{1/3}, \\ p_y &= \left(\frac{E |\sin \varphi|}{g} \right)^{2/3} - E \cos \varphi, \\ \text{where } 0 \leq \varphi \leq 2\pi, \quad E &\equiv \frac{\varepsilon}{\varepsilon_0}, \quad \varepsilon_0 = v^2/g_1. \end{aligned} \quad (4)$$

In this limit we calculate the Jacobian of the transformation, yielding the density of states as a function of energy ε :

$$\rho(\varepsilon) = \iint \frac{d^2 k}{(2\pi)^2} \delta(\varepsilon - \varepsilon(\mathbf{k})) = \frac{0.123}{g^{1/3} g_1} \left(\frac{\varepsilon}{\varepsilon_0} \right)^{1/3}. \quad (5)$$

We find the non-linear transformation Eq. (4) to be particularly elegant and effective in rendering the problem analytically tractable in the low-energy limit.

Perturbation Theory and Renormalization Group—We take into account the non-retarded Coulomb interaction $V(\mathbf{k}) = 2\pi e^2/|\mathbf{k}|$ to first order in perturbation theory. The self-energy is $\hat{\Sigma}(\mathbf{k}) = i/(2\pi)^3 \int_{-\infty}^{\infty} d\nu \int d^2 k' \hat{G}(\mathbf{k}', \nu) V(\mathbf{k} - \mathbf{k}')$, where $\hat{G}^{-1}(\mathbf{k}, \nu) = \nu - \mathcal{H}(\mathbf{k}) + i0^+ \text{sign}(\nu)$ is the fermionic Green's function. The frequency integral can be easily evaluated:

$$\hat{\Sigma}(\mathbf{k}) = \frac{1}{2} \int \frac{d^2 k'}{(2\pi)^2} \frac{2\pi e^2}{|\mathbf{k} - \mathbf{k}'|} \frac{1}{|\varepsilon(\mathbf{k}')|} \mathcal{H}(\mathbf{k}'). \quad (6)$$

As usual, we introduce the dimensionless coupling $\alpha = e^2/v$ ($\hbar = 1$). We calculate corrections to the quasiparticle velocity (v), mass (g_1), and cross anisotropy (g_2),

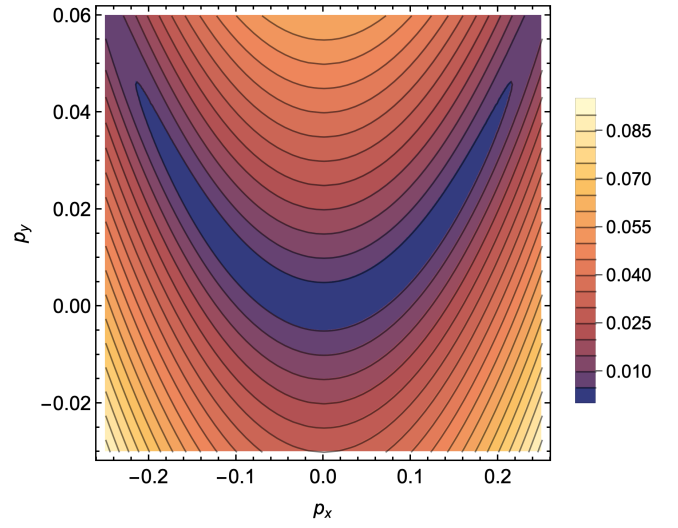


FIG. 2. Contour plot of the critical low energy spectrum Eq.(2), illustrated schematically in Figure 1b). Energies are measured in units of $\varepsilon_0 = v^2/g_1$ and momenta in units of v/g_1 . We take $g = 1/2$, similar to the cross anisotropy in the candidate material. The isoenergy curves have a characteristic boomerang shape.

which result in the following universal Hamiltonian, omitting cutoff dependent terms:

$$\begin{aligned} \tilde{\mathcal{H}}(\mathbf{k}) &= [g_1(1 + \Sigma_{g_1})k_x^2 - v(1 + \Sigma_v)k_y] \hat{\sigma}_x \\ &+ g_2(1 + \Sigma_{g_2})k_x k_y \hat{\sigma}_y. \end{aligned} \quad (7)$$

Details of the computation are outlined in the Supplementary Material (SM). We have the following one-loop perturbation theory results:

$$\begin{aligned} v(\omega) &= vL(\omega), \quad g_{1,2}(\omega) = g_{1,2}L(\omega), \\ L(\omega) &= \left(1 + \frac{\alpha}{\pi} \ln(\Lambda/\omega) \right), \end{aligned} \quad (8)$$

where Λ is a high energy cutoff, and the infrared $\omega \equiv \omega(\mathbf{k})$ is on-shell i.e. follows the form of the bare dispersion.

Next, we write down and integrate the corresponding Renormalization Group (RG) equations, where we introduce $\ell = \ln(\Lambda/\omega)$: $dv/d\ell = v\alpha/\pi = e^2/\pi$, $dg_1/d\ell = \alpha g_1/\pi$, $dg_2/d\ell = \alpha g_2/\pi$. These equations integrate to the final results, identical to Eq.(8). From the first equation we see that the coupling constant is marginally irrelevant, similarly to graphene [20]: $\alpha(\omega) = \alpha/(1 + \frac{\alpha}{\pi} \ln(\Lambda/\omega))$.

Effective Hamiltonian (Hartree-Fock level)— In addition to the logarithmic corrections, there appear two finite, cutoff-dependent contributions to the self-energy, Δ and c .

$$\mathcal{H}(\mathbf{k}) = (g_1 L(\omega) k_x^2 - v L(\omega) k_y + \alpha \Delta) \hat{\sigma}_x + (g_2 L(\omega) k_x k_y + \alpha c k_x) \hat{\sigma}_y. \quad (9)$$

We find $\Delta > 0$ which implies a shift of the dispersion in the k_y direction, meaning that the band crossing is now at $k_y = (g_1^2/v g_2)\alpha\Delta$ (whereas $\Delta < 0$ would have meant the presence of three Dirac cones, see Figure 1). More importantly, there is an interaction-generated linear term around the shifted semi-Dirac point $\sim \alpha ((g_1 g_2/v^3)\Delta + (g_1/v^2)c) k_x$ which indicates that the dispersion is effectively anisotropic Dirac at small momenta. As shown in Figure 3 the spectrum smoothly transitions from linear Dirac to type-II semi-Dirac behavior with increasing energy. To capture this crossover, we model the density of states for the interacting fermions as $\rho(\varepsilon) \sim \varepsilon^{\eta(\varepsilon)}$. A computation of $\eta(\varepsilon)$ for varying interaction strengths yields the results in Figure 4. The crossover from linear to semi-Dirac is clearly reflected in the decrease of η from 1 to the saturation at $1/3$. The onset is controlled by an interaction dependent energy scale corresponding to

$$|k_x^*| \approx \frac{\alpha[(g_2/v)\Delta + c]}{g_1(\omega(k_x^*))}, \quad (10)$$

the regime where the quadratic term $\sim k_x^2$ begins to dominate over the linear k_x term in Eq.(9). At small energies the renormalization (increase) of g_1 favors the semi-Dirac spectrum and suppresses the linear regime. In contrast, the running of g_1 under Coulomb interactions in ordinary semi-Dirac fermions gives rise to a linear spectrum for a large window of intermediate energies, with the renormalized semi-Dirac behavior present at the lowest energies [3].

Polarization Function and Random Phase Approximation—Going beyond the first order perturbative level, we introduce static screening via the Random Phase Approximation (RPA). We have evaluated the zero frequency polarization function numerically and have found that it is well-approximated by the form:

$$|\Pi(\mathbf{p})| = \left[c_1 (|p_x|^{1/2})^w + c_2 (|p_y|^{1/3})^w \right]^{1/w}, \quad w \gg 1 \quad (11)$$

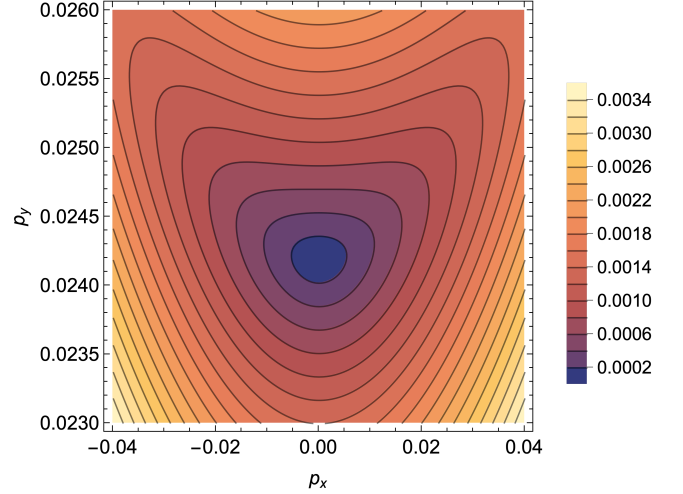


FIG. 3. Type-II semi-Dirac spectrum renormalized by the bare Coulomb interaction at the one-loop Hartree-Fock level for $\alpha = 0.2$ and $g = 1/2$. The convex lowest energy contours indicate an anisotropic Dirac cone, with concave semi-Dirac behavior appearing at higher energies corresponding to Eq.(10). An ultraviolet momentum cutoff $|k_{\Lambda}^{x,y}| = 1.1$ on a square region, in units of v/g_1 , is used to find the values $\Delta/\varepsilon_0 = 1.88/4\pi$ and $c/v = 1.39/4\pi$.

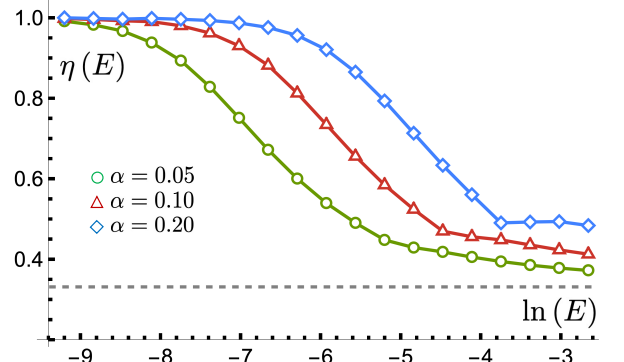


FIG. 4. Evolution of the power $\eta(E)$ in the density of states $\rho(E) \sim E^{\eta(E)}$ for $g = 1/2$ under different interaction strengths $\alpha = 0.05, 0.10, 0.20$ at the Hartree-Fock level. The smooth transition from linear Dirac behavior $\eta = 1$ at the smallest energies, approaching type-II semi-Dirac behavior $\eta = 1/3$ (dashed line) with increasing energy, captures the variation in the interacting spectrum shown in Figure 3.

implying the following structure:

$$|\Pi(\mathbf{p})| = \begin{cases} c_1 |p_x|^{1/2}, & \frac{c_2 |p_y|^{1/3}}{c_1 |p_x|^{1/2}} \leq 1 \\ c_2 |p_y|^{1/3}, & \frac{c_2 |p_y|^{1/3}}{c_1 |p_x|^{1/2}} \geq 1 \end{cases} \quad (12)$$

The number of fermionic species is taken to be $N = 4$. The boundary between the two regions is visible in the plot of the polarization in Figure 5.

The self-energy is then calculated using the dressed

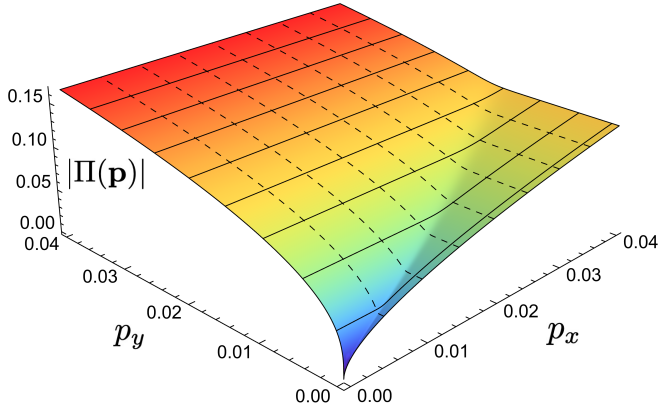


FIG. 5. Static polarization function for type-II semi-Dirac fermions. The ravine residing on $p_y = (c_1/c_2)^3 p_x^{3/2}$ demarcates two regions where the polarization is dominated by $\sqrt{p_x}$ and $p_x^{1/3}$ dependence, and flat in the other direction. The dashed and solid mesh lines at constant p_x, p_y exhibit this structure. Values of $c_1 = 0.196\pi$ and $c_2 = 0.154\pi$ were calculated, and $w = 50$ was used for illustration.

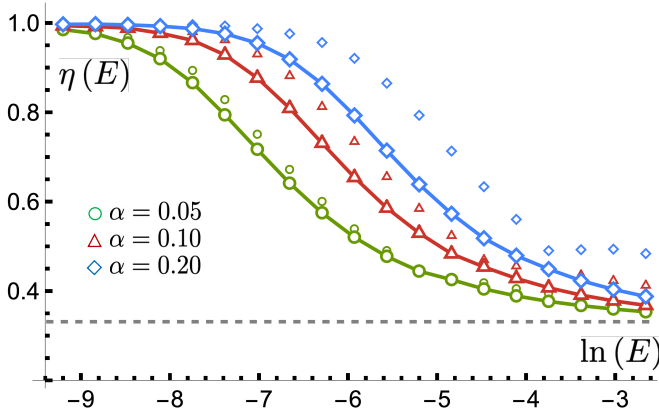


FIG. 6. Evolution of the density of states scaling $\eta(E)$ under the RPA screened Coulomb interaction (solid curves) for $g = 1$. We have included the corresponding Hartree-Fock results, given by the smaller unconnected markers, for comparison. For the interaction strengths $\alpha = 0.05, 0.10, 0.20$ values of $\Delta/\varepsilon_0 = 1.83/(4\pi), 1.55/(4\pi), 1.19/(4\pi)$ and $c/v = 1.39/(4\pi), 1.19/(4\pi), 0.93/(4\pi)$ are calculated respectively in the RPA. At the HF level the values $\Delta/\varepsilon_0 = 1.89/(4\pi)$ and $c/v = 1.71/(4\pi)$ ($g = 1$) are independent of α . Results are qualitatively similar, with the smaller values of η under the RPA indicating a weaker renormalization as expected.

Coulomb potential $V_{RPA}(\mathbf{p}) = V(\mathbf{p})/(1 - V(\mathbf{p})\Pi(\mathbf{p}))$ and the variation in the renormalized density of states is summarized in Figure 6. While results are qualitatively similar to their HF counterparts, it is evident that introducing screening naturally inhibits the bare interaction effects, suppressing enhancement of the spectrum. Note that Δ, c are now functions of α , and in fact decay with increasing interaction strength, partially neutralizing the growth of the crossover energy scale with α . Details of

the numerical self-energy fits are given in the SM.

Implications for Scaling of Physical Observables. Conclusions and Discussion—The change of electronic dispersion has profound implications for the behavior of various characteristics at low temperatures/energies. As the density of states evolves between powers $\eta = 1$ at the lowest energies and $\eta = 1/3$ for higher energies (non-interacting quasiparticles), the specific heat evolves from $C_V(T) \sim T^2$ ($\eta = 1$), to $C_V(T) \sim T^{4/3}$ ($\eta = 1/3$). In general: $C_V(T) \sim T^{\eta+1}$.

The electronic compressibility κ is defined as: $\kappa^{-1} = n^2(\partial\mu/\partial n)$ and can be probed experimentally [20–23]. Here μ is the chemical potential and n the electronic density ($n \sim \mu^{\eta+1}$). $\partial\mu/\partial n$ is the inverse density of states. The charge response is typically determined by $\partial\mu/\partial n$ which is related to the inverse capacitance. One finds $\partial\mu/\partial n \sim 1/\mu \sim 1/\sqrt{n}$ ($\eta = 1$), and $\partial\mu/\partial n \sim 1/\mu^{1/3} \sim 1/n^{1/4}$ ($\eta = 1/3$). In general: $\partial\mu/\partial n \sim 1/\mu^\eta \sim 1/n^{\eta/(\eta+1)}$.

Landau level quantization [14, 15, 21, 24, 25] is governed by the semi-classical formula $A(\varepsilon_n(B)) = \int_0^{\varepsilon_n(B)} \rho(\omega) d\omega \sim nB$, where $A(\varepsilon) = \int_{\varepsilon(\mathbf{k}) \leq \varepsilon} d^2\mathbf{k}/(2\pi)^2$ is the area enclosed by the energy dispersion in momentum space. Thus we find $\varepsilon_n(B) \sim \pm[nB]^{1/(\eta+1)}$. In particular for the non-interacting fermions, $\varepsilon_n(B) \sim \pm[nB]^{3/4}$ presents a unique signature for experimental detection. The scaling is distinct from the conventional $B^{2/3}$ in type-I semi-Dirac systems, and there is a zero energy Landau level due to the finite Berry phase. Note that the conventional magnetic field dependence may be mimicked by interacting type-II fermions under suitable conditions.

Transport coefficients, such as dynamical conductivity, can be sensitive to the geometry of the Fermi surface [26]. In our case the shape evolves from convex to concave (boomerang) from low to high energy (Figure 3), with an expected associated change in the conductivity's frequency dependence. We expect that the conclusions reached in this work will remain valid for finite, small particle density (i.e. small filling of the upper band). Similarly to graphene the charge is not renormalized, as reflected in the non-singular behavior of the polarization function. Topological characteristics, such as the Chern number and the anomalous Hall conductivity, are not affected by the interactions. Overall the interacting Dirac liquid is anticipated to behave as a Fermi liquid but with the remarkable evolution of the Fermi surface shape as a function of the long-range interaction, implying a density of states evolution from linear to power one-third and corresponding changes in the Landau levels quantization condition. Can these effects be detected in real materials? We would suggest, for example, that the modification of the interaction strength α by using dielectric screening (i.e. $e^2 \rightarrow e^2/\kappa$), could potentially probe the interaction exponent presented in Figures (4), (6).

Acknowledgements—We thank Dmitrii Maslov and

Bruno Uchoa for stimulating discussions. Partial financial support provided by the University of Vermont is gratefully acknowledged.

[1] G. Montambaux, F. Piéchon, J.-N. Fuchs, and M. O. Goerbig, Merging of Dirac points in a two-dimensional crystal, *Phys. Rev. B* **80**, 153412 (2009).

[2] G. Montambaux, F. Piéchon, J.-N. Fuchs, and M. Goerbig, A universal Hamiltonian for motion and merging of Dirac points in a two-dimensional crystal, *The European Physical Journal B* **72**, 509 (2009).

[3] M. M. Elsayed, B. Uchoa, and V. N. Kotov, Coulomb interactions in systems of generalized semi-Dirac fermions, *Phys. Rev. B* **111**, 165127 (2025).

[4] B. Roy and M. S. Foster, Quantum Multicriticality near the Dirac-Semimetal to Band-Insulator Critical Point in Two Dimensions: A Controlled Ascent from One Dimension, *Phys. Rev. X* **8**, 011049 (2018).

[5] M. M. Elsayed and V. N. Kotov, Microscopic lattice model for quartic semi-Dirac fermions in two dimensions, *Journal of Physics: Condensed Matter* **37**, 315501 (2025).

[6] H. Huang, Z. Liu, H. Zhang, W. Duan, and D. Vanderbilt, Emergence of a Chern-insulating state from a semi-Dirac dispersion, *Phys. Rev. B* **92**, 161115 (2015).

[7] V. Pardo and W. E. Pickett, Metal-insulator transition through a semi-Dirac point in oxide nanostructures: VO_2 (001) layers confined within TiO_2 , *Phys. Rev. B* **81**, 035111 (2010).

[8] Z. Liao, H. Zeng, E. Wang, and H. Huang, Berry Curvature Dipole and Nonlinear Hall Effect in Type-II Semi-Dirac Systems, *Small* **1**, 2409691 (2025).

[9] Y.-W. Son, S.-M. Choi, Y. P. Hong, S. Woo, and S.-H. Jhi, Electronic topological transition in sliding bilayer graphene, *Phys. Rev. B* **84**, 155410 (2011).

[10] J.-N. Chen, Y.-Y. Yang, Y.-L. Zhou, Y.-J. Wu, H.-J. Duan, M.-X. Deng, and R.-Q. Wang, Photon-modulated linear and nonlinear anomalous Hall effects in type-II semi-Dirac semimetals, *Phys. Rev. B* **105**, 085124 (2022).

[11] Q.-Y. Xiong, J.-Y. Ba, H.-J. Duan, M.-X. Deng, Y.-M. Wang, and R.-Q. Wang, Optical conductivity and polarization rotation of type-II semi-Dirac materials, *Phys. Rev. B* **107**, 155150 (2023).

[12] Y. Shao, S. Moon, A. N. Rudenko, J. Wang, J. Herzog-Arbeitman, M. Ozerov, D. Graf, Z. Sun, R. Queiroz, S. H. Lee, Y. Zhu, Z. Mao, M. I. Katsnelson, B. A. Bernevig, D. Smirnov, A. J. Millis, and D. N. Basov, Semi-Dirac Fermions in a Topological Metal, *Phys. Rev. X* **14**, 041057 (2024).

[13] P. Dietl, F. Piéchon, and G. Montambaux, New Magnetic Field Dependence of Landau Levels in a Graphenelike Structure, *Phys. Rev. Lett.* **100**, 236405 (2008).

[14] M. Goerbig and G. Montambaux, Dirac Fermions in Condensed Matter and Beyond, in *Dirac Matter*, edited by B. Duplantier, V. Rivasseau, and J.-N. Fuchs (Springer International Publishing, 2017) pp. 25–53.

[15] R. de Gail, J.-N. Fuchs, M. Goerbig, F. Piéchon, and G. Montambaux, Manipulation of Dirac points in graphene-like crystals, *Physica B: Condensed Matter* **407**, 1948 (2012).

[16] V. N. Kotov, B. Uchoa, and O. P. Sushkov, Coulomb interactions and renormalization of semi-Dirac fermions near a topological Lifshitz transition, *Phys. Rev. B* **103**, 045403 (2021).

[17] B. Uchoa and K. Seo, Superconducting states for semi-Dirac fermions at zero and finite magnetic fields, *Phys. Rev. B* **96**, 220503 (2017).

[18] M. D. Uryszek, E. Christou, A. Jaefari, F. Krüger, and B. Uchoa, Quantum criticality of semi-Dirac fermions in 2 + 1 dimensions, *Phys. Rev. B* **100**, 155101 (2019).

[19] H. Isobe, B.-J. Yang, A. Chubukov, J. Schmalian, and N. Nagaosa, Emergent Non-Fermi-Liquid at the Quantum Critical Point of a Topological Phase Transition in Two Dimensions, *Phys. Rev. Lett.* **116**, 076803 (2016).

[20] V. N. Kotov, B. Uchoa, V. M. Pereira, F. Guinea, and A. H. Castro Neto, Electron-Electron Interactions in Graphene: Current Status and Perspectives, *Rev. Mod. Phys.* **84**, 1067 (2012).

[21] S. M. Girvin and K. Yang, *Modern Condensed Matter Physics* (Cambridge University Press, 2019).

[22] J. Martin, N. Akerman, G. Ulbricht, T. Lohmann, J. H. Smet, K. von Klitzing, and A. Yacoby, Observation of electron-hole puddles in graphene using a scanning single-electron transistor, *Nature Physics* **4**, 144 (2007).

[23] D. E. Sheehy and J. Schmalian, Quantum Critical Scaling in Graphene, *Phys. Rev. Lett.* **99**, 226803 (2007).

[24] A. A. Abrikosov, *Fundamentals of the Theory of Metals* (North-Holland, 1988).

[25] G. P. Mikitik and Y. V. Sharlai, Manifestation of Berry's Phase in Metal Physics, *Phys. Rev. Lett.* **82**, 2147 (1999).

[26] D. L. Maslov and A. V. Chubukov, Optical response of correlated electron systems, *Reports on Progress in Physics* **80**, 026503 (2016).